International Journal of Greenhouse Gas Control 5 (2011) 788–797

Contents lists available at ScienceDirect

International Journal of Greenhouse Gas Control

journal homepage: www.elsevier.com/locate/ijggc

Determining the corrosive potential of CO_2 transport pipeline in high pCO_2–water environments

Yoon-Seok Choi*, Srdjan Nešić

Institute for Corrosion and Multiphase Technology, Department of Chemical and Biomolecular Engineering, Ohio University, Athens, OH 45701, USA

ARTICLE INFO

Article history:
Received 27 July 2010
Received in revised form 8 November 2010
Accepted 15 November 2010
Available online 13 December 2010

Keywords:
CO_2 transport pipeline
Supercritical CO_2
Thermodynamic modeling
CO_2 corrosion
Carbon steel

ABSTRACT

The corrosive potential of carbon steel was evaluated under high pressure CO_2–water systems to simulate the condition of CO_2 transportation pipeline in the CO_2 capture and storage (CCS) applications. To understand the thermodynamic properties of CO_2–water systems related to the corrosion phenomena, thermodynamic modeling were conducted to determine the mutual solubilities of CO_2 and water in the two coexisting phases, and to calculate the concentrations of corrosive species in the free water at various pressures and temperatures. Carbon steel samples were exposed to water-saturated CO_2, and CO_2-saturated water in the CO_2 pressure range of 40–80 bar at 50 °C. The corrosion rate of samples was determined by weight loss measurements. The surface morphology and the composition of the corrosion product layers were analyzed by using surface analytical techniques (SEM and EDS).

1. Introduction

Emissions from fossil fuel-fired power plants represent a significant source of carbon dioxide (CO_2) emissions, a known greenhouse gas. The capture and storage of CO_2 in geological reservoirs is now considered to be one of the main options for achieving deep reductions in greenhouse gas emissions (Rubin et al., 2005; Connell, 2005). The CO_2 capture and storage (CCS) process involves three stages: capture of the CO_2 from the power plant or industrial process, transmission of the CO_2 to the storage site followed by injection into the geological reservoir (Gale and Davison, 2004). In order to avoid two-phase flow regimes and increase the density of the CO_2, the captured CO_2 gas is typically compressed to the supercritical state while the temperature and the pressure are over 31.1 °C and 73.8 bar, respectively, thereby making it easier and less costly to transport (Gale and Davison, 2004; Kruse and Tekiela, 1996). The research activities are largely concentrating on development of the capture technology to reduce costs, and on assessing the technical feasibility of injecting and monitoring the CO_2 within the geological reservoirs themselves (Stevens and Gale, 2000). Little of the research is being conducted on CO_2 transmission, but this remains a critical component that should not be overlooked.

Low alloy carbon steel pipelines have been used for transportation of CO_2 at high pressure, but in all cases, CO_2 must be dried to eliminate the corrosion risk (Seiersten and Kongshaug, 2005). However, if CO_2 transport is to be achieved at a large scale or in existing pipelines, it will not be practical to dry it sufficiently and liquid water "breakout" is to be expected. Furthermore, drying CO_2 contributes to an increase in handling cost, especially for offshore installations where weight allowance and space for process equipment installation are very restricted (Kongshaug and Seiersten, 2004). When free water exists in the pipeline, it will be saturated with CO_2 and the corrosion rate will be significant for carbon steel because of the formation of carbonic acid (H_2CO_3). In addition, even though pure, dry CO_2 is not corrosive, there are several studies which provide qualitative evidence for corrosion on carbon steel in water-saturated supercritical CO_2 phase (Russick et al., 1996; Propp et al., 1996; McGrail et al., 2009). Thus, to be able to consider the corrosion risk in such pipelines, quantitative evaluation of corrosion in both CO_2-saturated water and water-saturated CO_2 phases will be needed.

The impact of CO_2 corrosion on carbon steel has been studied extensively at pressures relevant for oil and gas transport (up to 20 bar CO_2). At higher pressures experimental data are sparse. Since CO_2 changes from gaseous to liquid or supercritical with increasing pressure, it will lead to different interactions with water, i.e., CO_2 solubility in water will not follow Henry's law in liquid or supercritical CO_2 conditions, which results in changing water chemistry. Since the solubility of water in CO_2 is related to the free-liquid water formation and the solubility of CO_2 in water correlates with the corrosive potential of free water, accurate estimations of the mutual solubilities of CO_2 and water are an important issue in CO_2 transportation pipeline corrosion. Although many studies have been done to model mutual solubilities of CO_2

* Corresponding author. Tel.: +1 740 593 9944; fax: +1 740 593 9949.
E-mail address: choiy@ohio.edu (Y.-S. Choi).

1750-5836/$ – see front matter © 2010 Elsevier Ltd. All rights reserved.
doi:10.1016/j.ijggc.2010.11.008

and water at high pressures, there is no attempt to predict the water chemistry at such a high pressure.

Thus, in the present study, to understand the thermodynamic properties of CO_2–water systems related to observed corrosion phenomena, thermodynamic modeling studies were conducted to determine the mutual solubilities of CO_2 and water in the two coexisting phases, and to calculate the concentrations of corrosive species in the free-liquid water at various ranges of pressure and temperature (up to 300 bar, 85 °C). In addition, the corrosion properties with increasing pressure were investigated for carbon steel by weight loss measurements and surface analysis techniques.

2. Thermodynamic modeling

The thermodynamic model used in this work was based on a combination of mutual solubilities of CO_2 and water (Spycher et al., 2003), and chemistry of water-rich phase (Nordsveen et al., 2003).

2.1. Modeling for mutual solubilities of the CO_2–water system

Spycher et al. (2003) reviewed the published experimental P-T-x data for the CO_2–water system in the temperature range of 12–100 °C at pressures up to 600 bar to develop a solubility model. They used a non-iterative procedure to calculate the composition of the compressed CO_2 and liquid phase at equilibrium based on equating chemical potentials and using the Redlich–Kwong (RK) equation of state (EOS) (Redlich and Kwong, 1949). Their procedure is kept as simple as possible and is suitable for our purpose to establish a preliminary thermodynamic model to predict the mutual solubilities of CO_2 and water in high pressure CO_2 pipeline applications. In the following, an approach for calculating the mutual solubilities of CO_2 and water is presented using the Spycher model.

At equilibrium in the CO_2–water system, the following equilibria and equations to define relationships can be written:

$$H_2O_{(g)} \leftrightarrow H_2O_{(l)} \tag{1}$$

$$K_{H_2O} = \frac{f_{H_2O(g)}}{a_{H_2O(l)}} \tag{2}$$

$$CO_{2(g)} \leftrightarrow CO_{2(aq)} \tag{3}$$

$$K_{CO_2} = \frac{f_{CO_2(g)}}{a_{CO_2(aq)}} \tag{4}$$

where K is true equilibrium constants, f is fugacity of the gas components, and a is activity of components in the liquid phase. The K values for water and CO_2 are functions of pressure and temperature as:

$$K_{(T,P)} = K^0_{(T,P^0)} \exp\left(\frac{(P-P^0)\bar{V}_i}{RT}\right) \tag{5}$$

where P, P^0, R, T are pressure, reference pressure (1 bar), gas constant and temperature in K, respectively. $\bar{V}_i$ is the average partial molar volume of the pure component i over the pressure interval P^0 to P.

From the definition of fugacity ($f_i = \varnothing_i y_i P$) (Prausnitz et al., 1986), the mole fraction of water in the CO_2 phase (y_{H_2O}) can be written by combining Eqs. (2) and (5):

$$y_{H_2O} = \frac{K^0_{H_2O} a_{H_2O}}{\varnothing_{H_2O} P} \exp\left(\frac{(P-P^0)\bar{V}_{H_2O}}{RT}\right) \tag{6}$$

where, $\varnothing_{H_2O}$ is the fugacity coefficient of water.

Table 1
Element analysis for the X65 carbon steel used in the tests (wt.%).

C	Mn	Si	P	S	Cr	Cu	Ni	Mo	Al
0.065	1.54	0.25	0.013	0.001	0.05	0.04	0.04	0.007	0.041

Fig. 1. The test autoclave used for corrosion experiments.

For better accuracy at high pressures, the water activity deviation from unity caused by dissolved CO_2 should be taken into account. Using Raoult's law, the water activity can be approximated by its mole fraction in the water phase ($x_{H_2O} = 1 - x_{CO_2}$), such that:

$$y_{H_2O} = \frac{K^0_{H_2O}(1-x_{CO_2})}{\varnothing_{H_2O} P} \exp\left(\frac{(P-P^0)\bar{V}_{H_2O}}{RT}\right) \tag{7}$$

where, x_{CO_2} is the mole fraction of CO_2 in the water phase. There is the following relationship between a_{CO_2} and x_{CO_2}:

$$a_{CO_2} = 55.508 x_{CO_2} \tag{8}$$

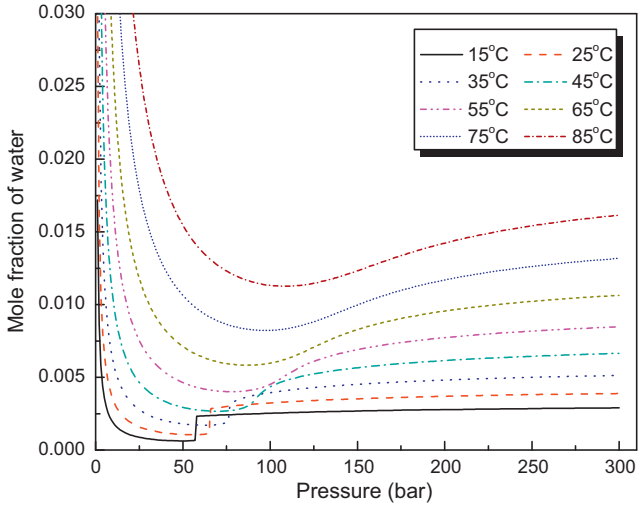

Fig. 2. Calculated solubility of water in CO_2 as functions of pressure and temperature.

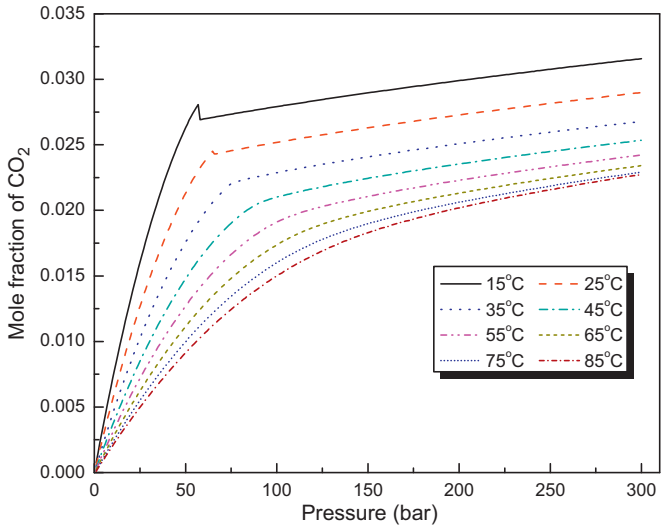

Fig. 3. Calculated solubility of CO_2 in water as functions of pressure and temperature.

Substituting Eqs. (5) and (8) into Eq. (4) gives:

$$x_{CO_2} = \frac{\varnothing_{CO_2}(1 - y_{H_2O})P}{55.508K^0_{CO_2(g)}} \exp\left(-\frac{(P - P^0)\bar{V}_{CO_2}}{RT}\right) \quad (9)$$

Eqs. (7) and (9) can be solved directly by setting:

$$A = \frac{K^0_{H_2O}}{\varnothing_{H_2O}P_{tot}} \exp\left(\frac{(P - P^0)\bar{V}_{H_2O}}{RT}\right) \quad (10)$$

$$B = \frac{\varnothing_{CO_2}P_{tot}}{55.508K^0_{CO_2(g)}} \exp\left(-\frac{(P - P^0)\bar{V}_{CO_2}}{RT}\right) \quad (11)$$

Using parameters A and B, we can calculate the mole fraction of water in the CO_2 phase (y_{H_2O}) and the mole fraction of CO_2 in the water phase (x_{CO_2}) as follows:

$$y_{H_2O} = \frac{(1 - B)}{((1/A)B)} \quad (12)$$

$$x_{CO_2} = B(1 - y_{H_2O}) \quad (13)$$

The average partial molar volume of the pure water ($\bar{V}_{H_2O} = 18.1\,cm^3/mol$) and CO_2 ($\bar{V}_{CO_2(g)} = 32.6\,cm^3/mol$, $\bar{V}_{CO_2(l)} - 32\,cm^3/mol$), and the K parameters were obtained from the literature and/or by calibration to the solubility data:

$$\log K^0_{H_2O} = -2.209 + 3.097 \times 10^{-2}T - 1.098 \times 10^{-4}T^2 + 2.048 \times 10^{-7}T^3 \quad (14)$$

$$\log K^0_{CO_2(g)} = 1.189 + 1.304 \times 10^{-2}T - 5.446 \times 10^{-5}T^2 \quad (15)$$

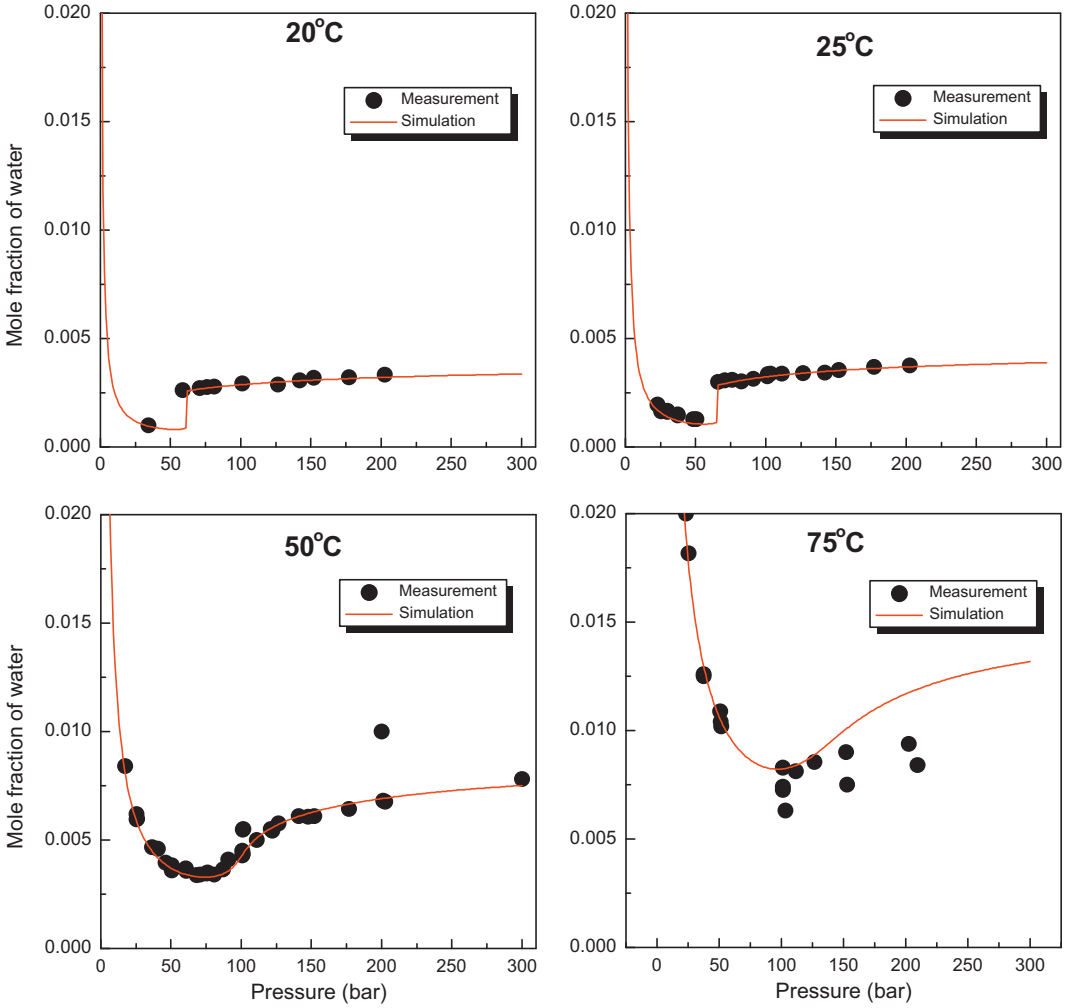

Fig. 4. Comparison between experimental data (Wiebe, 1941; Coan and King, 1971; Song and Kobayashi, 1987; Briones et al., 1987; King et al., 1992; Bamberger et al., 2000) and calculated water solubility in CO_2 at various pressures and temperatures.

$$\log K^0_{CO_2(l)} = 1.169 + 1.368 \times 10^{-2}T - 5.380 \times 10^{-5}T^2 \quad (16)$$

where T is temperature in °C.

The fugacity coefficients in Eqs. (10) and (11) should be derived from an equation of state (EOS) which can calculate properties of CO_2–water mixtures. In this study, Redlich–Kwong (RK) EOS was used to get the fugacity coefficients and the volume of the compressed gas phase. The RK EOS is given by (Redlich and Kwong, 1949):

$$P = \left(\frac{RT}{V-b}\right) - \left(\frac{a}{T^{0.5}V(V+b)}\right) \quad (17)$$

where V is the molar volume of the CO_2-rich phase at pressure P and temperature T, and R is the gas constant. Parameters a and b characterize intermolecular attraction and repulsion, respectively.

For CO_2–water mixtures, the mixture constants a_{mix} and b_{mix} can be calculated by the standard mixing rules:

$$a_{mix} = \sum_{i=1}^{n}\sum_{j=1}^{n} y_i y_j a_{ij} = y^2_{H_2O}a_{H_2O} + 2y_{H_2O}y_{CO_2}a_{H_2O\text{–}CO_2} + y^2_{CO_2}a_{CO_2} \quad (18)$$

$$b_{mix} = \sum_{i=1}^{n} y_i b_i = y_{H_2O}b_{H_2O} + y_{CO_2}b_{CO_2} \quad (19)$$

From these mixing rules and Eq. (17), the fugacity coefficient of component k in mixture with other component i can be calculated as:

$$\ln(\varnothing_k) = \ln\left(\frac{V}{V-b_{mix}}\right) + \left(\frac{b_k}{V-b_{mix}}\right) - \left(\frac{2\sum_{i=1}^{n} y_i a_{ik}}{RT^{1.5}b_{mix}}\right)\ln\left(\frac{V+b_{mix}}{V}\right) + \left(\frac{a_{mix}b_k}{RT^{1.5}b^2_{mix}}\right) \times \left[\ln\left(\frac{V+b_{mix}}{V}\right) - \left(\frac{b_{mix}}{V+b_{mix}}\right)\right] - \ln\left(\frac{PV}{RT}\right) \quad (20)$$

To avoid an iterative scheme, the assumption of infinite water dilution in the CO_2-rich phase is made that $y_{H_2O} = 0$ and $y_{CO_2} = 1$ in the mixing rules in Eqs. (18) and (19). Then, a_{mix} and b_{mix} can be replaced to a_{CO_2} and b_{CO_2} in Eq. (20), respectively. And the volume of the compressed gas phase (V) can be calculated by recasting RK EOS in terms of volume:

$$V^3 - V^2\left(\frac{RT}{P}\right) - V\left(\frac{RTb_{CO_2}}{P} - \frac{a_{CO_2}}{PT^{0.5}} + b^2_{CO_2}\right) - \left(\frac{a_{CO_2}b_{CO_2}}{PT^{0.5}}\right) = 0 \quad (21)$$

where, $R = 83.1447\ \text{bar cm}^3\ \text{mol}^{-1}\ \text{K}^{-1}$, V is in cm^3/mol, P is in bar, and T is in K.

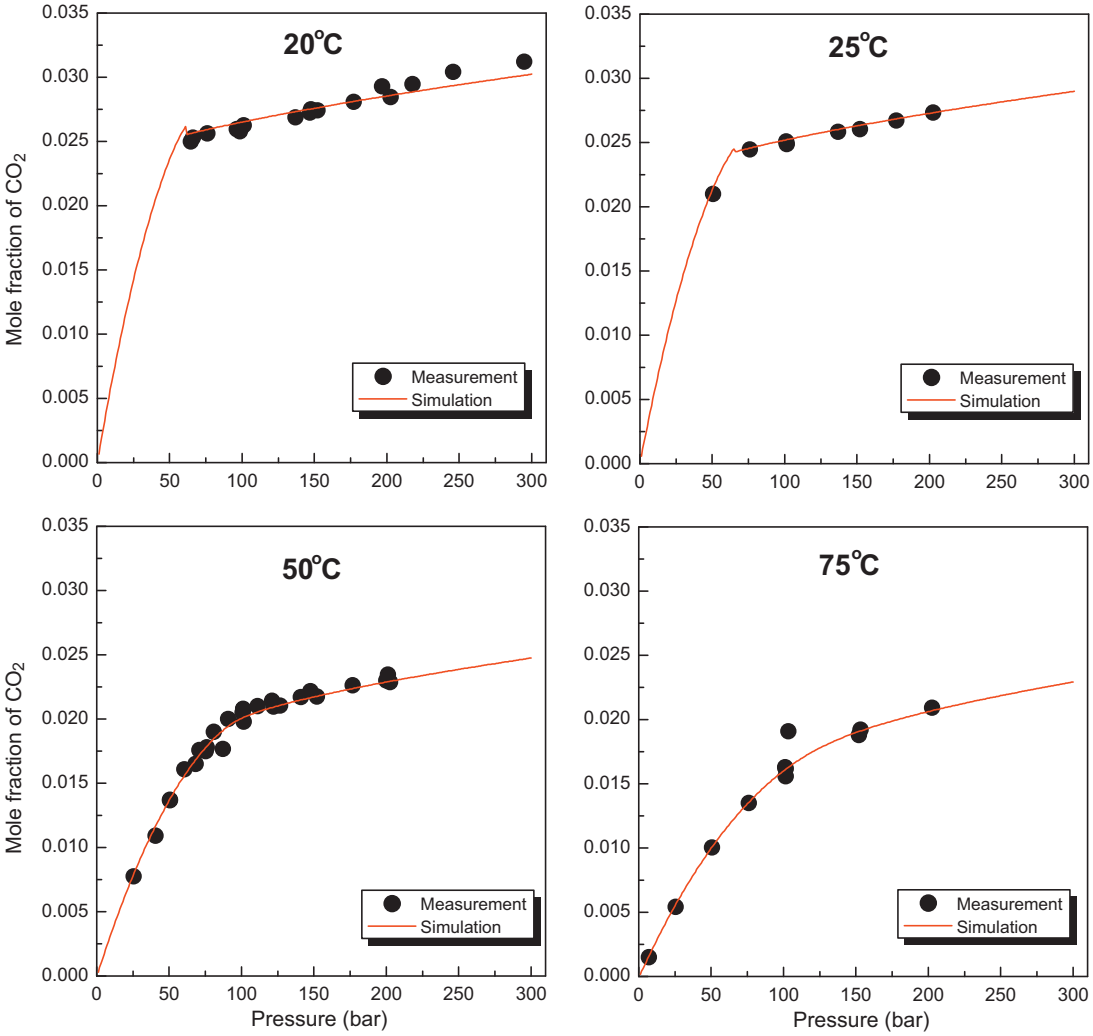

Fig. 5. Comparison between experimental data (Wiebe, 1941; Coan and King, 1971; Song and Kobayashi, 1987; Briones et al., 1987; King et al., 1992; Bamberger et al., 2000) and calculated CO_2 solubility in water at various pressures and temperatures.

A FORTRAN program was used to calculate the mutual solubilities of CO_2 and water in the temperature range of 15–85 °C and pressure up to 300 bar.

2.2. Modeling for the chemistry of free water and for the prediction of $FeCO_3$ precipitation

Understanding water chemistry is an important precondition for predicting corrosion under high CO_2 pressure. The concentrations of carbonic species ($CO_{2(aq)}$, H_2CO_3, HCO_3^-, and CO_3^{2-}) as well as autogenous pH in the water phase were calculated to provide a tool for estimating water chemistry of a pipeline when water precipitates using the solubility of CO_2 and equilibrium constants for each chemical reaction at various pressure and temperature ranges. In the case of CO_2 transporting pipelines, due to a virtually unlimited supply of CO_2, there is constant partial pressure of CO_2 on the surface of free water so that the system can be considered as an 'open' system.

Once CO_2 dissolves in water (Eq. (3)), $CO_{2(aq)}$ is involved in a sequence of chemical reactions as follows:

$$CO_{2(aq)} + H_2O \overset{K_{hyd}}{\longleftrightarrow} H_2CO_3 \text{ (Hydration of aqueous } CO_2\text{)} \quad (22)$$

$$H_2CO_3 \overset{K_{ca}}{\longleftrightarrow} H^+ + HCO_3^- \text{ (Dissociation of carbonic acid)} \quad (23)$$

$$HCO_3^- \overset{K_{bi}}{\longleftrightarrow} H^+ + CO_3^{2-} \text{ (Dissociation of bicarbonate ion)} \quad (24)$$

$$H_2O \overset{K_w}{\longleftrightarrow} H^+ + OH^- \text{ (Dissociation of water)} \quad (25)$$

With the partial pressure of CO_2 known in an open system, Henry's law can be applied in order to calculate the vapor–liquid equilibrium of CO_2 at low pressure (Brown et al., 2003). However, at high pressure, Henry's law cannot be used to calculate the concentration of CO_2 in the solution. Thus, in the present study, the concentrations of CO_2 in the water (C_{CO_2}) were calculated using the solubility of CO_2 in water (x_{CO_2}) obtained from Eq. (13).

Once concentration of dissolved CO_2 is fixed, the reactions shown above can be described by equilibria reactions as follows based on the assumption of infinite dilution:

$$K_{hyd} = \frac{C_{H_2CO_3}}{C_{CO_2} C_{H_2O}} \quad (26)$$

$$K_{ca} = \frac{C_{H^+} C_{HCO_3^-}}{C_{H_2CO_3}} \quad (27)$$

$$K_{bi} = \frac{C_{H^+} C_{CO_3^{2-}}}{C_{HCO_3^-}} \quad (28)$$

$$K_w = \frac{C_{H^+} C_{OH^-}}{C_{H_2O}} \quad (29)$$

where $C_{H_2CO_3}$, $C_{HCO_3^-}$, $C_{CO_3^{2-}}$, C_{H^+}, and C_{OH^-} are the concentrations (mol/L) of carbonic acid, bicarbonate ion, carbonate ion, hydrogen ion, and hydroxide ion, respectively.

The equilibrium constants, K, are a function of the temperature and are available in the open literature (Nordsveen et al., 2003). Since the solution cannot have a net charge, an electroneutrality relation is required. Mathematically, it is expressed as:

$$C_{H^+} = C_{HCO_3^-} + 2 \times C_{CO_3^{2-}} C_{OH^-} \quad (30)$$

FORTRAN and Excel programs were used to calculate the concentrations of species in the solution with various temperature and pressure ranges.

3. Materials and methods

The test specimens were machined from API X65 low carbon steel with a size of 25 mm × 15 mm × 3 mm. The composition of this steel is given in Table 1. The specimens were ground with 600 grit silicon carbide paper, cleaned with alcohol in an ultrasonic bath, dried, and weighed using a balance with a precision of 0.1 mg. The electrolyte used in this work was DI water.

The weight loss experiments were performed in a 2000 psi static autoclave with 1000 ml volume (Fig. 1). 400 ml of solution was added to the autoclave and CO_2 gas was bubbled for 3 h to remove oxygen before starting the test. Corrosion tests were conducted under different partial pressures of CO_2 (pCO_2, 40–80 bar) at 50 °C. When both water and CO_2 are added in the autoclave, there is a phase separation with the water phase at the bottom. Specimens were inserted both in the water-saturated CO_2 phase at the top of the autoclave and in the CO_2-saturated water phase at the bottom.

The corrosion rates were determined from weight-loss method at the end of a 24-h exposure. The specimens were removed and cleaned for 5 min in Clarke solution (20 g antimony trioxide + 50 g stannous chloride and hydrochloric acid to make 1000 ml) (ASTM G1, 2003). The specimens were then rinsed in distilled water, dried and weighed to 0.1 mg. The corrosion rate can be calculated by the

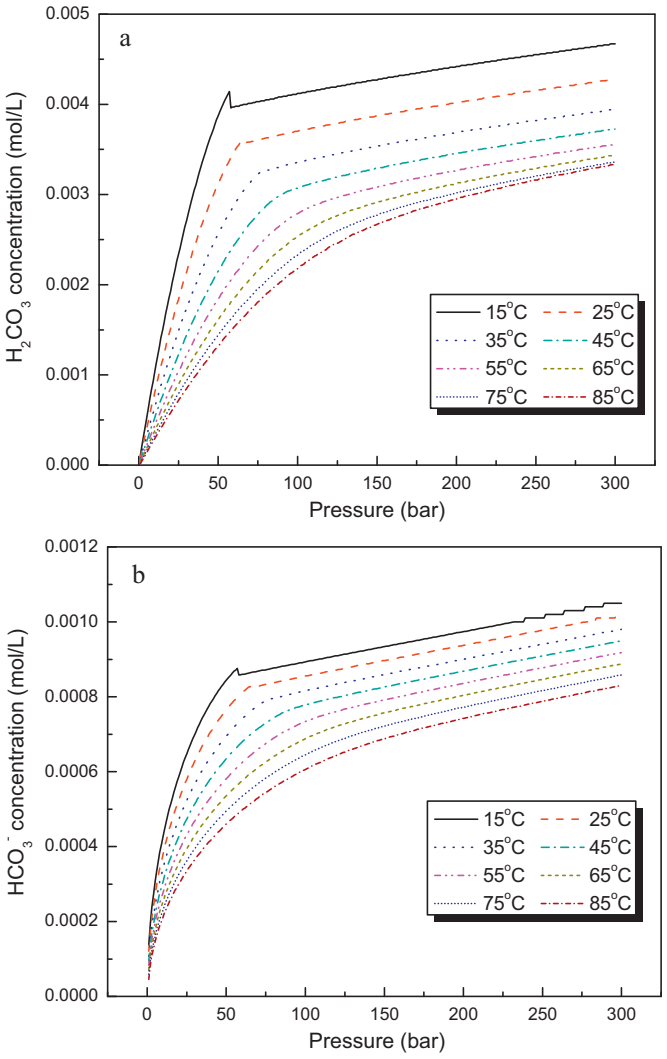

Fig. 6. Variations of (a) H_2CO_3 and (b) HCO_3^- concentrations as functions of pressure and temperature obtained from the water chemistry model.

following equation (ASTM G31, 1994):

$$\text{Corrosion rate (mm/y)} = \frac{8.76 \times 10^4 \times \text{weight loss (g)}}{\text{area (cm}^2) \times \text{density (g/cm}^3) \times \text{time (h)}} \quad (31)$$

The morphology and compositions of corrosion products were analyzed by scanning electron microscopy (SEM) and energy dispersive X-ray spectroscopy (EDS).

4. Results and discussion

4.1. Thermodynamic modeling

The mutual solubilities of CO_2 and water calculated using Eqs. (12) and (13) are shown in Figs. 2 and 3 in terms of mole fractions of water and CO_2. The solubility of water in CO_2 showed high values at low pressures, passes through a minimum, and then increased with pressure. The discontinuity in water solubility at subcritical temperatures (15, 25 °C) coincides with the phase change from a gaseous to a liquid CO_2. Above the critical temperature (31.1 °C), it is related to the phase change from a gaseous to a supercritical CO_2 after which the trend with pressure becomes smoother. However, the solubility of CO_2 in water increased sharply with rising pressure up to the saturation pressure and at a lesser rate thereafter. The CO_2 solubility trend with pressure reflected two solubility curves for two distinct phases: liquid or supercritical CO_2 above saturation pressure, and gaseous CO_2 below this pressure. This resulted in a break in slope on the overall solubility trends.

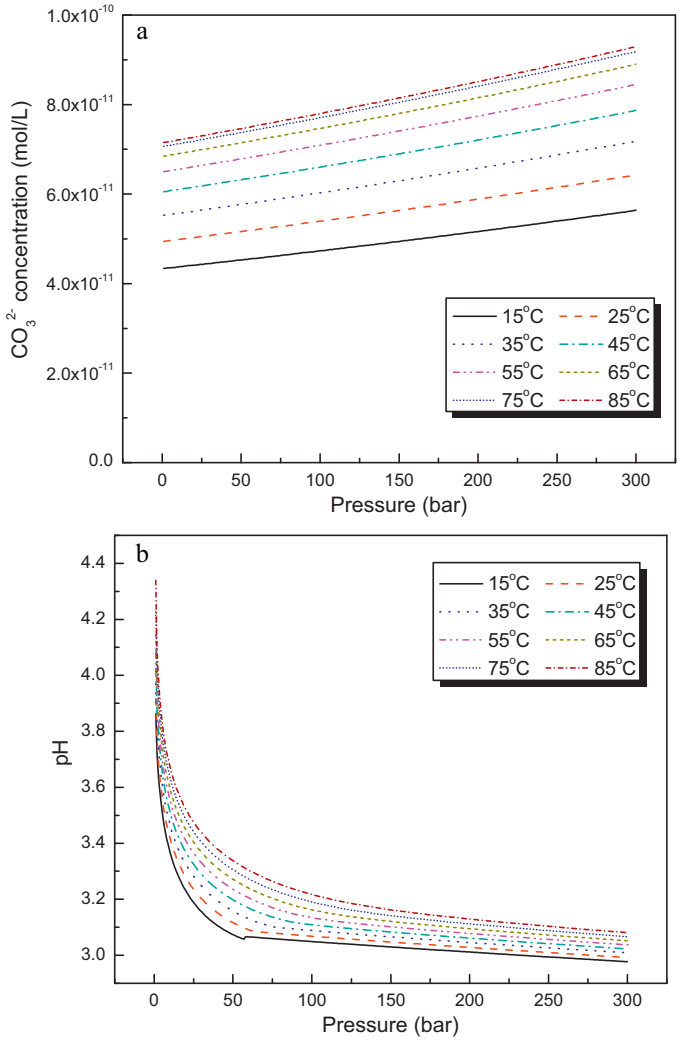

Fig. 7. Variations of (a) CO_3^{2-} concentration and (b) pH as functions of pressure and temperature obtained from the water chemistry model.

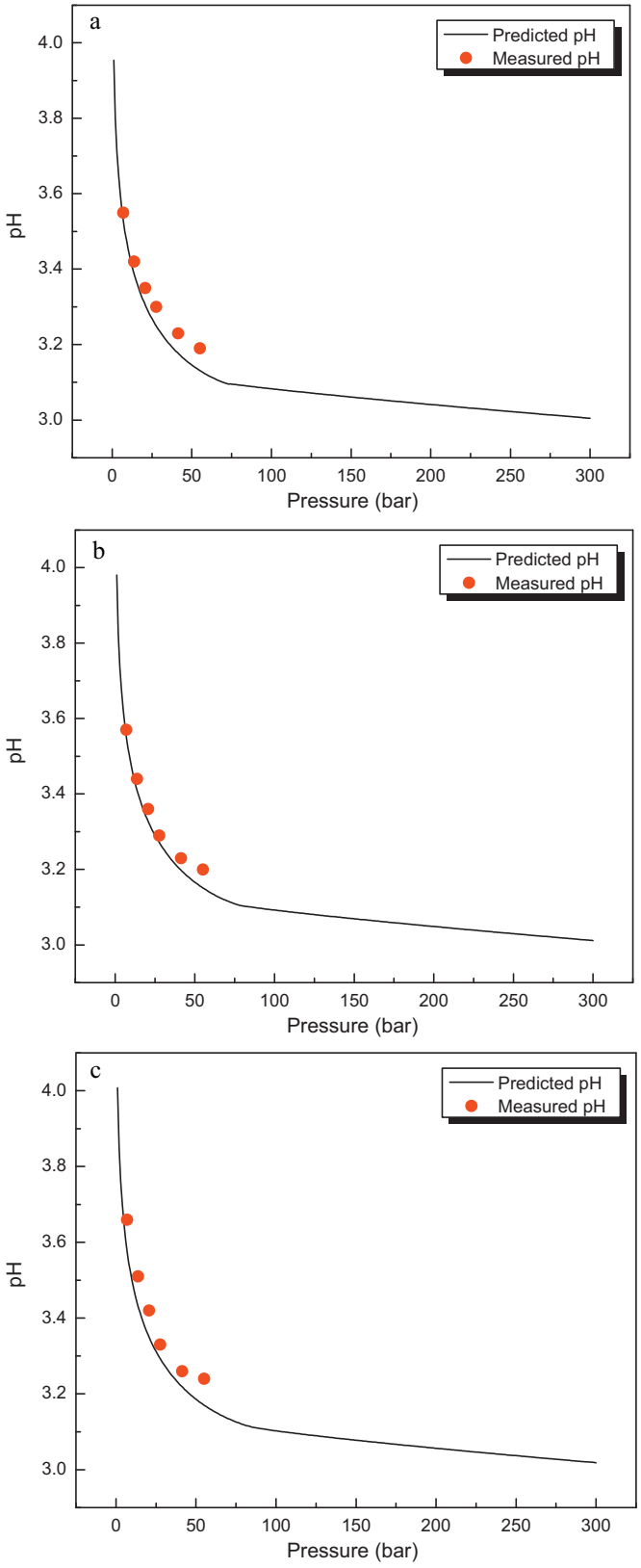

Fig. 8. Comparison between experimental data (Meyssami et al., 1992) and calculated pH at various pressures and temperatures: (a) 32 °C, (b) 37 °C, and (c) 42 °C.

The effects of temperature on the solubility of water and on the solubility of CO_2 are significantly different, and the solubility of water increased while the solubility of CO_2 decreased with increase in temperature. This behavior of the CO_2–water system is due probably to changes in compressibility of CO_2 and hydration of water (Teng and Yamasaki, 2002), e.g., at 80 bar the density of CO_2 is 707.2 kg/m^3 at T = 30 °C and becomes 966 kg/m^3 at T = 0 °C, indicating that the resistance for water to penetrate into CO_2 decreases with increasing temperature; in comparison, water density varies with temperature only slightly, and the effect of hydration, which enhances the dissolution of CO_2 in water is greater at low temperature than at high temperatures.

Fig. 4 shows a comparison between the predicted solubility of water in CO_2 and that from experimental data available in the literature (Wiebe, 1941; Coan and King, 1971; Song and Kobayashi, 1987; Briones et al., 1987; King et al., 1992; Bamberger et al., 2000). The comparison demonstrates an acceptable match in the temperature range of 15–50 °C, however, calculated water solubility has less accuracy at higher temperatures, because the water mole fractions in the CO_2 phase keeps increasing with temperature so that the assumption of infinite water dilution should eventually break down (Spycher et al., 2003). A comparison between solubility of CO_2 in water calculated using the model versus the experimental data (Wiebe, 1941; Coan and King, 1971; Song and Kobayashi, 1987; Briones et al., 1987; King et al., 1992; Bamberger et al., 2000) is represented in Fig. 5. Results presented in this figure show a good agreement at various temperatures and pressures.

The effects of pressure and temperature on the concentrations of carbonic species (H_2CO_3, HCO_3^-, and CO_3^{2-}) and pH (H^+) are shown in Figs. 6 and 7. The concentrations of H_2CO_3 and HCO_3^- showed the same trends as the solubility of CO_2 in water shown in Fig. 3, i.e., the concentrations increased with increasing pressure whereas decreased with temperature. However, the concentration of CO_3^{2-} increased with increasing pressure and temperature. The pH values changed in the range of 4.4–3, decreasing with an increase in pressure and increasing with temperature. The autogenous pH of free water will be in the range of 3.1–3.3 under supercritical CO_2 condition (P > 73 bar, T > 31.1 °C), which can lead to a more acidic environment compared with atmospheric conditions (pH 3.9 at 1 bar, 25 °C). At such low pH values, the solubility of iron carbonate is sufficiently high that no precipitate would be observed (scale-free CO_2 corrosion).

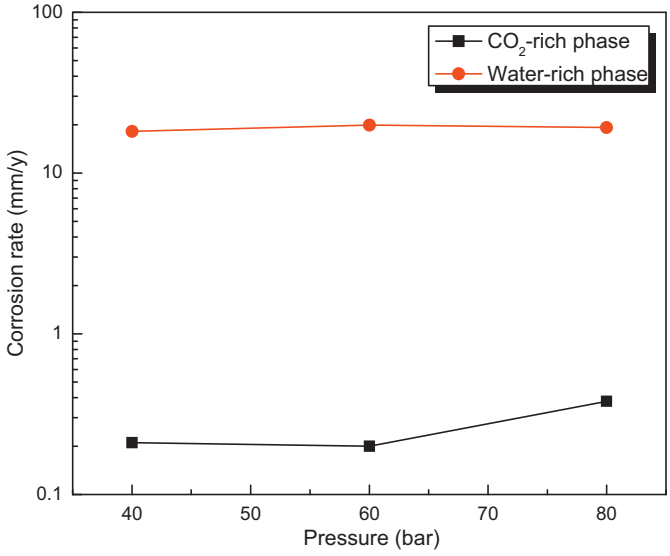

Fig. 9. Measured corrosion rates in the CO_2-saturated water and the water-saturated CO_2 phases at 50 °C as a function of CO_2 partial pressure.

The measured (Meyssami et al., 1992) and predicted pH values are plotted in Fig. 8. It can be found that the thermodynamic model closely predicted the pH at different pressures and temperatures.

4.2. Corrosion tests under high pCO_2–water system

Fig. 9 shows the corrosion rates of carbon steel in the CO_2-saturated water phase and the water-saturated CO_2 phase under different pCO_2 after 24 h at 50 °C. Note that the CO_2 phase was gaseous at 40 and 60 bar, whereas it was supercritical at 80 bar. As shown in Fig. 9, the corrosion rates of carbon steel in the CO_2-saturated water phase are much higher than in the water-saturated CO_2 phase. The corrosion rates of carbon steel in the CO_2-saturated water were in the range of 18–20 mm/y and the increase of pCO_2

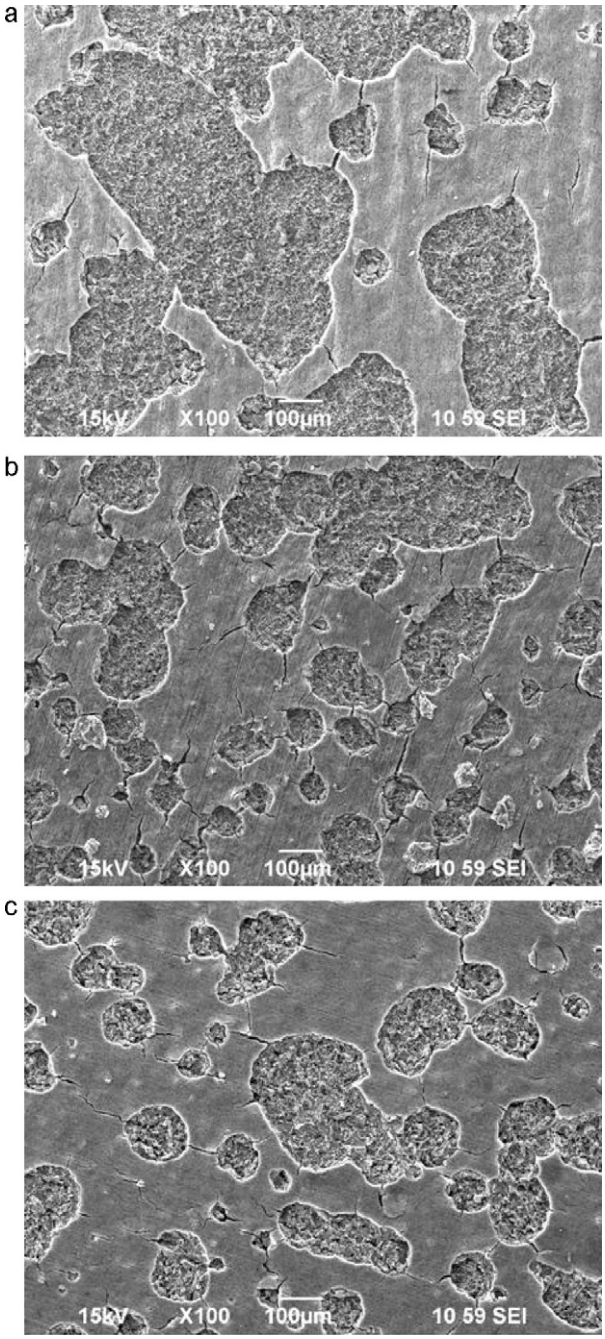

Fig. 10. SEM images of the corroded surface of samples exposed to the CO_2-saturated water for 24 h with different pCO_2: (a) 40 bar, (b) 60 bar, and (c) 80 bar.

in the system did not significantly increase the corrosion rates of carbon steel. A similar high corrosion rate was reported for carbon steel at 82 bar pCO_2, 80 °C (Cui et al., 2004). The commonly accepted explanation for the effect of pCO_2 on the corrosion rate is that with pCO_2 the concentration of H_2CO_3 increases and accelerates the cathodic reaction (Eq. (32)) and ultimately the corrosion rate (Nesic, 2007).

$$2H_2CO_3 + 2e^- \rightarrow H_2 + 2HCO_3^- \quad (32)$$

Based on the water chemistry predicted in Fig. 6(a), the concentrations of H_2CO_3 in these experiments would be 1.67 mM (40 bar), 2.26 mM (60 bar), and 2.68 mM (80 bar). Compared with the concentration at 1 bar (0.044 mM), it increases almost 60 times with changing pCO_2 from 1 bar to 80 bar, whereas pH changes from 4.05 (1 bar) to 3.14 (80 bar) (Fig. 7(b)). This agrees with the finding (Wang et al., 2004) that the anodic reaction is practically unaffected when the pCO_2 is increased from 3 to 20 bar while the cathodic limiting current density is strongly increased due to the dominant effect of H_2CO_3.

Fig. 10 shows the surface morphologies of the corroded samples in the CO_2-saturated water phase at different pressures. It can be seen that the morphologies were almost identical with different pressures and the surface was locally covered by the corrosion products. Fig. 11 represents the SEM image and EDS spectra of the sample surface exposed to the CO_2-saturated water phase at 80 bar and 50 °C. The corrosion product consists mainly of iron carbide (Fe_3C) and constituents of some alloying elements from the carbon steel (area A), whereas the uncovered region was identified as steel substrate with trace amounts of carbon and oxygen (area B). The Fe_3C initially presents in the carbon steel, reveals after the preferential dissolution of ferrite (α-Fe) and accumulates on the steel surface, therefore it is non-protective, porous and easily peels off from the substrate (Kermani and Morshed, 2003). Fig. 12 shows the surface morphologies of samples in the CO_2-saturated water phase under different pCO_2 after cleaning with Clarke solution. As shown in Fig. 12, uniform corrosion attack was observed on the surface for all samples, i.e., no localized corrosion. This implies that even though the Fe_3C film locally formed on the steel surface,

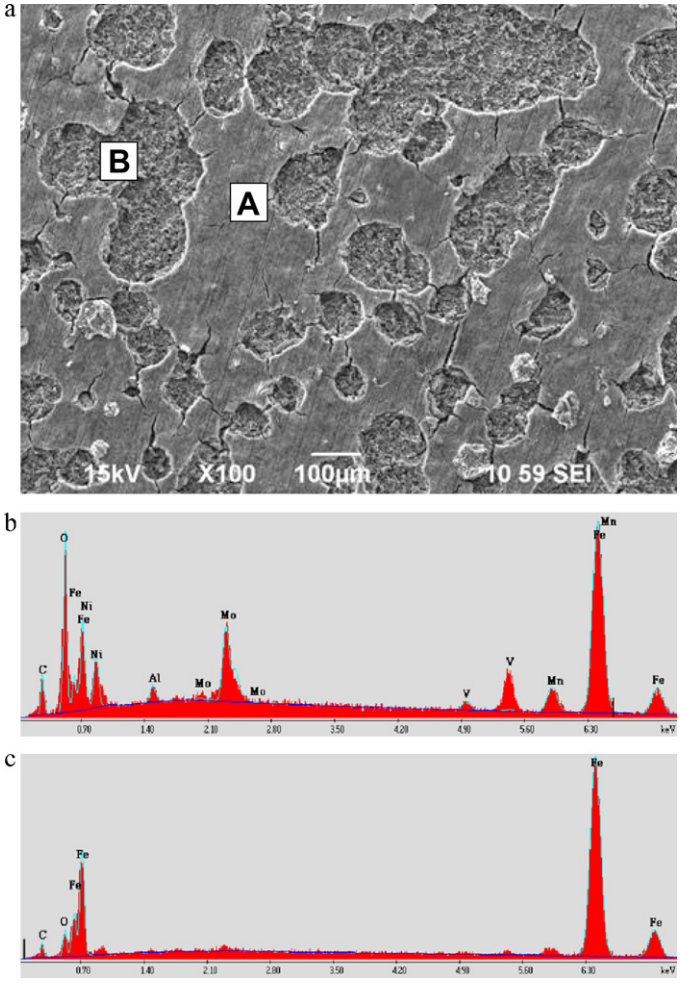

Fig. 11. SEM image and EDS spectra of the corroded surface of samples exposed to the CO_2-saturated water for 24 h at 80 bar pCO_2 and 50 °C: (a) SEM image, (b) EDS spectrum of area A, and (c) EDS spectrum of area B.

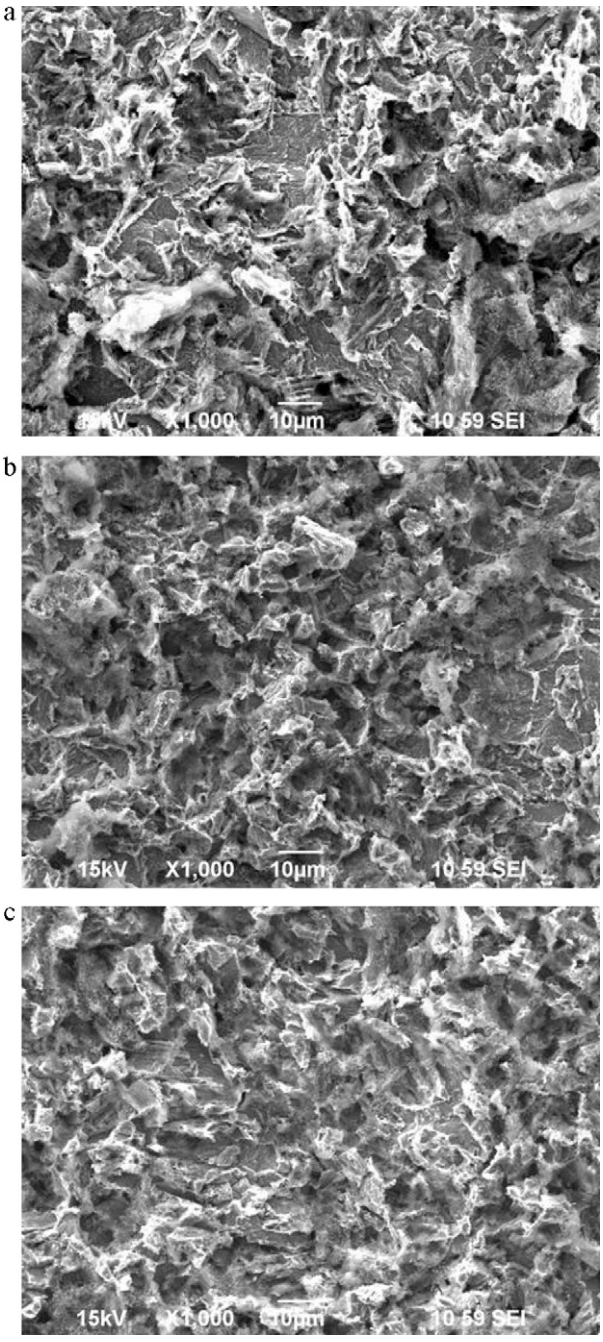

Fig. 12. SEM images of the corroded surface of samples exposed to the CO_2-saturated water for 24 h with different pCO_2 (after cleaning): (a) 40 bar, (b) 60 bar, and (c) 80 bar.

it did not initiate localized corrosion due to the non-protective nature of Fe_3C film.

Fig. 13 shows the SEM images and EDS spectra of the sample surface after 24 h in the water-saturated CO_2 phase with different pressures. It is interesting to note that the sample surfaces were covered by corrosion products after 24 h in the CO_2-rich phase even though there was no free-water on the sample surface at the initial stage. SEM and EDS analysis showed that the surface was covered by dense, crystalline iron carbonate ($FeCO_3$), and the grain size of $FeCO_3$ decreased with increasing pressure. This indicates that corrosion can take place in the water-saturated CO_2 phase under high pCO_2 conditions, but the corrosion rate is low (~0.2 mm/y) due to the formation of $FeCO_3$ on the steel surface. This may be explained by the condensation of water from the CO_2 phase due to pressure or temperature changes during the experiment. Since the CO_2 phase was saturated by water, it is very likely that dissolved water can condense with small changes of pressure and temperature. Once the water condenses on the steel surface, it will become immediately saturated with CO_2 so that $FeCO_3$ can precipitate on the steel surface and further reduce the corrosion reaction.

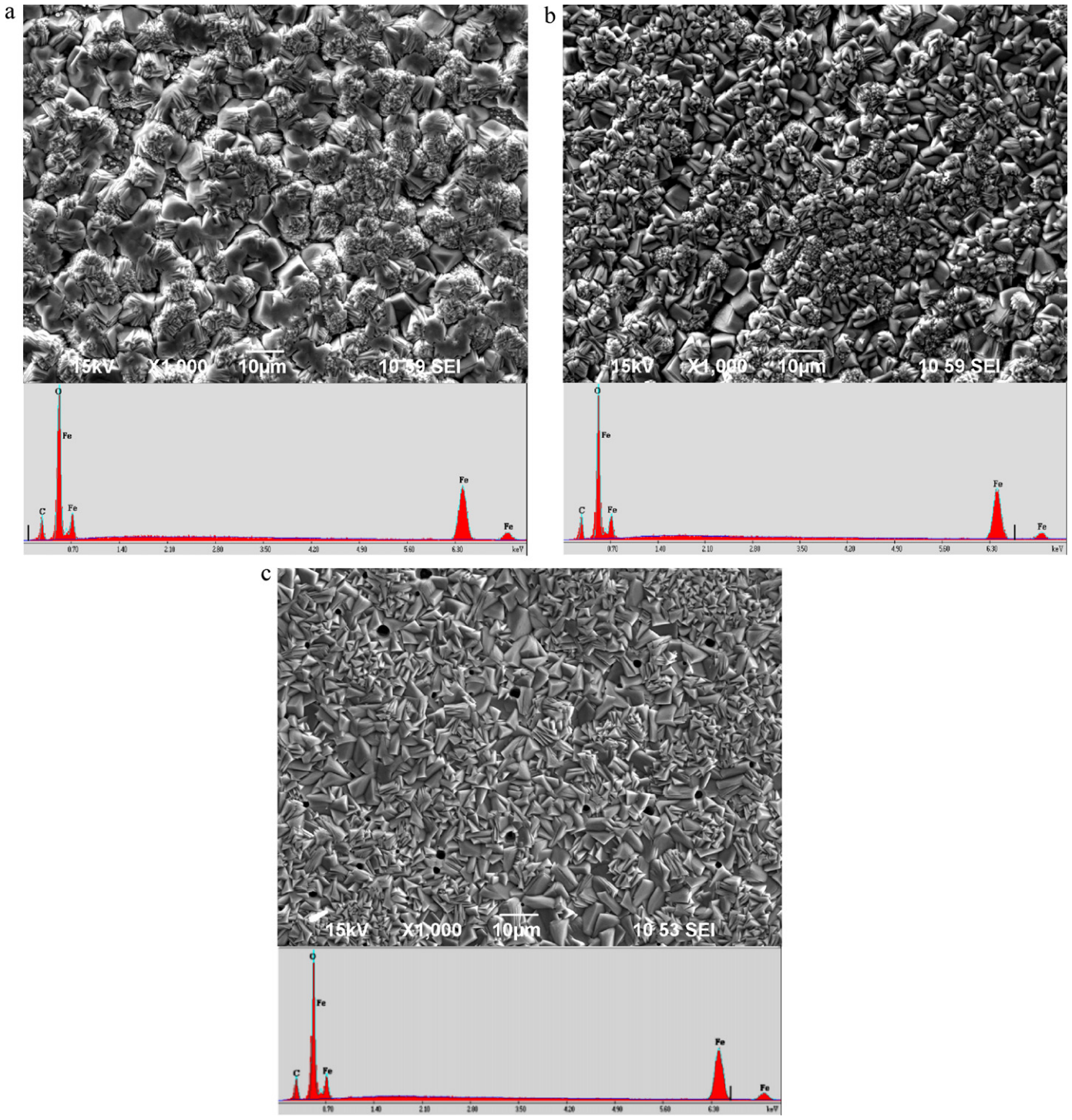

Fig. 13. SEM images and EDS spectra of the corroded surface of samples exposed to the water-saturated CO_2 for 24 h with different pCO_2: (a) 40 bar, (b) 60 bar, and (c) 80 bar.

5. Conclusions

The mutual solubilities of CO_2 and water, and the chemistry of the free water over wide ranges of temperature and pressure, were predicted by thermodynamic modeling. In addition, the corrosion properties with increasing pressure were investigated for carbon steel in both CO_2-saturated water and water-saturated CO_2 phases by weight loss measurements and surface analysis techniques. The following conclusions are drawn:

- The solubility of water in CO_2 and the solubility of CO_2 in water increased with increasing pressure, however, the solubility of CO_2 in water was much larger than that of water in CO_2.
- The solubility of water in CO_2 increased while the solubility of CO_2 in water decreased with an increase in temperature.
- The calculated water solubility in CO_2 showed good agreement between the calculated and experimental data at low and medium temperatures, and up to 300 bar of pressure. When temperature was above 75 °C, there were significant discrepancies.
- The calculated CO_2 solubility in water from 15 to 85 °C, and up to 300 bar, showed a good agreement with experimental data.
- The concentrations of $CO_{2(aq)}$, H_2CO_3 and HCO_3^- increased with increasing pressure but decreased with an increase in temperature. The concentration of CO_3^{2-} increased linearly with increasing pressure and temperature, and the pH value changed in the range of 4.4–3 which decreased with an increase in pressure and increased with increasing temperature.
- The corrosion rates of carbon steel in the CO_2-saturated water were very high but did not significantly change with pressure from 40 to 80 bar.
- Corrosion can take place in the water-saturated CO_2 phase under high pressure conditions when no free water is present, but the corrosion rate was low (~0.2 mm/y) due to the formation of $FeCO_3$ on the steel surface.

Acknowledgments

The authors would like to acknowledge the financial support from Ohio Coal Development Office (OCDO) for the Institute for Corrosion and Multiphase Technology at Ohio University.

References

ASTM Standard G1-03, 2003. Standard practice for preparing, cleaning, and evaluating corrosion test specimens. In: Annual Book of ASTM Standards, vol. 03. 02, ASTM International, West Conshohocken, PA.

ASTM Standard G 31, 1994. Standard practice for laboratory immersion corrosion testing of metals. In: Annual Book of ASTM Standards, vol. 03. 02, ASTM International, West Conshohocken, PA.

Bamberger, A., Sieder, G., Maurer, G., 2000. High-pressure (vapor + liquid) equilibrium in binary mixtures of (carbon dioxide + water or acetic acid) at temperatures from 313 to 353 K. The Journal of Supercritical Fluids 17, 97–110.

Briones, J.A., Mullins, J.C., Thies, M.C., Kim, B.U., 1987. Ternary phase equilibria for acetic acid–water mixtures with supercritical carbon dioxide. Fluid Phase Equilibria 36, 235–246.

Brown, B., Lee, K.-L.J., Nesic, S., 2003. Corrosion in multiphase flow containing small amounts of H_2S, CORROSION/2003. NACE, Houston, TX, Paper No. 03341.

Coan, C.R., King, A.D., 1971. Solubility of water in compressed carbon dioxide, nitrous oxide, and ethane. Evidence for hydration of carbon dioxide and nitrous oxide in the gas phase. Journal of the American Chemical Society 93 (8), 1857–1862.

Connell, D.P., 2005. Carbon Dioxide Capture Options for Large Point Sources in the Midwestern United States: An Assessment of Candidate Technologies, Final Report. CONSOL Energy Inc., South Park, PA.

Cui, Z.D., Wu, S.L., Li, C.F., Zhu, S.L., Yang, X.J., 2004. Corrosion behavior of oil tube steels under conditions of multiphase flow saturated with super-critical carbon dioxide. Materials Letters 58, 1035–1040.

Gale, J., Davison, J., 2004. Transmission of CO_2-safety and economic considerations. Energy 29, 1319–1328.

Kermani, M.B., Morshed, A., 2003. Carbon dioxide corrosion in oil and gas production – a compendium. Corrosion 59, 659–683.

King, M.B., Mubarak, A., Kim, J.D., Bott, T.R., 1992. The mutual solubilities of water with supercritical and liquid carbon dioxide. The Journal of Supercritical Fluids 5, 296–302.

Kongshaug, K.O., Seiersten, M., 2004. Baseline experiments for the modelling of corrosion at high CO_2 pressure, CORROSION/2004. NACE, Houston, TX, Paper No. 04630.

Kruse, H., Tekiela, M., 1996. Calculating the consequences of a CO_2-pipeline rupture. Energy Conversion and Management 37, 1013–1018.

McGrail, B.P., Schaef, H.T., Glezakou, V.-A., Dang, L.X., Owen, A.T., 2009. Water reactivity in the liquid and supercritical CO_2 phase: has half the story been neglected? Energy Procedia 1, 3415–3419.

Meyssami, B., Balaban, M.O., Teixeira, A.A., 1992. Prediction of pH in model systems pressurized with carbon dioxide. Biotechnology Progress 8, 149–154.

Nesic, S., 2007. Key issues related to modelling of internal corrosion of oil and gas pipelines – a review. Corrosion Science 49, 4308–4338.

Nordsveen, M., Nesic, S., Nyborg, R., Stangeland, A., 2003. A mechanistic model for carbon dioxide corrosion of mild steel in the presence of protective iron carbonate films – part 1: theory and verification. Corrosion 59, 443–456.

Prausnitz, J.M., Lichtenthaller, R.N., De Azedevo, E.G., 1986. Molecular Thermodynamics of Fluid Phase Equilibria. Prentice Hall, New York, NY.

Propp, W.A., Carleson, T.E., Wai, C.M., Taylor, P.R., Daehling, K.W., Huang, S., Abdel-Latif, M., 1996. Corrosion in Supercritical Fluids. US Department of Energy report DE96014006, Washington DC.

Redlich, O., Kwong, J.N.S., 1949. On the thermodynamics of solutions. V. An equation of state. Fugacities of gaseous solutions. Chemical Reviews 44, 233–244.

Rubin, E., Meyer, L., Coninck, H., 2005. Carbon Dioxide Capture and Storage: Technical Summary. IPCC Special Report, p. 29.

Russick, E.M., Poulter, G.A., Adkins, C.L.J., Sorensen, N.R., 1996. Corrosive effects of supercritical carbon dioxide and cosolvents on metals. The Journal of Supercritical Fluids 9, 43–50.

Seiersten, M., Kongshaug, K.O., 2005. Materials selection for capture, compression, transport and injection of CO_2. In: Thomas, D.C., Benson, S.M. (Eds.), Carbon Dioxide Capture for Storage in Deep Geologic Formations, vol. 2. Elsevier Ltd., Oxford, UK, pp. 937–953.

Song, K.Y., Kobayashi, R., 1987. Water content of CO_2 in equilibrium with liquid water and/or hydrates. SPE Formation Evaluation, 500–508.

Spycher, N., Pruess, K., King, J.E., 2003. CO_2–H_2O mixtures in the geological sequestration of CO_2. I. Assessment and calculation of mutual solubilities from 12 to 100 °C and up to 600 bar. Geochimica et Cosmochimica Acta 67, 3015–3031.

Stevens, S.H., Gale, J., 2000. Geologic CO_2 sequestration. Oil and Gas Journal 98, 40–44.

Teng, H., Yamasaki, A., 2002. Pressure-mole fraction phase diagrams for CO_2–pure water system under temperatures and pressures corresponding to ocean waters at depth to 3000 m. Chemical Engineering Communications 189, 1485–1497.

Wang, S., George, K., Nesic, S., 2004. High pressure CO_2 corrosion electrochemistry and the effect of acetic acid, CORROSION/2004. NACE, Houston, TX, Paper No. 375.

Wiebe, R., 1941. The binary system carbon dioxide–water under pressure. Chemical Reviews 29, 475–481.